

Competing many-body instabilities in two-dimensional dipolar Fermi gases

Ahmet Keleş^{1,2} and Erhai Zhao²

¹*Department of Physics and Astronomy, University of Pittsburgh, Pittsburgh, PA 15260*

²*Department of Physics and Astronomy, George Mason University, Fairfax, VA 22030*

Experiments on quantum degenerate Fermi gases of magnetic atoms and dipolar molecules begin to probe their broken symmetry phases dominated by the long-range, anisotropic dipole-dipole interaction. Several candidate phases including the p -wave superfluid, the stripe density wave, and a supersolid have been proposed theoretically for two-dimensional spinless dipolar Fermi gases. Yet the phase boundaries predicted by different approximations vary greatly, and a definitive phase diagram is still lacking. Here we present a theory that treats all competing many-body instabilities in the particle-particle and particle-hole channel on equal footing. We obtain the low temperature phase diagram by numerically solving the functional renormalization-group flow equations and find a nontrivial density wave phase at small dipolar tilting angles and strong interactions, but no evidence of the supersolid phase. We also estimate the critical temperatures of the ordered phases.

Fermi gases and Fermi liquids play a fundamental role in many-body physics. Many archetypical broken symmetry phases ranging from superconductivity, charge density waves to quantum liquid crystals may be understood as instabilities of an underlying Fermi liquid in a particular interaction channel. Historically, electron gas with Coulomb interaction, liquid helium-3, and ultracold Fermi gases of alkali atoms with contact interaction have served as the testing grounds for many-body theories. Recent experiments have ushered in a new class of interacting Fermi gases — the quantum degenerate gases of fermionic atoms with large magnetic moments such as ^{161}Dy [1], ^{167}Er [2], and ^{53}Cr [3] and ground-state polar molecules such as $^{40}\text{K}^{87}\text{Rb}$ [4, 5] and $^{23}\text{Na}^{40}\text{K}$ [6–8]. Their low temperature phases are dictated by the dipole-dipole interaction which is long-ranged, anisotropic, and attractive or repulsive depending on the relative orientation of the two dipoles. This unique interaction gives rise to a rich variety of interesting quantum phases [9–11].

Take the single-species (spinless) dipolar Fermi gas confined in two dimensions (2D) for example. Previous theoretical work has identified two broken symmetry phases. A density wave (DW) is shown to develop when the dipolar interaction is repulsive, e.g. when the dipoles are aligned normal to the 2D plane by the external field, and sufficiently strong [12–18]. It features a periodic modulation of particle density in the form of unidirectional stripes. When the dipoles are tilted toward the plane beyond a critical angle, the dipolar interaction becomes partially attractive and supports Cooper pairing [19]. A broad region of Bardeen-Cooper-Schrieffer (BCS) superfluid phase with p -wave symmetry was predicted [20–22]. In the limit of large tilting angle and strong attraction, the system becomes unstable: the compressibility becomes negative and the gas is believed to collapse [12, 14, 20, 23]. While the qualitative picture of the competing DW and BCS instabilities is agreed upon, there is yet a consensus on a definitive phase diagram. For example, the DW instability is predicted to occur when the dimensionless interaction strength [defined below Eq.

(1)] $g_c = 1.45$ within the conserving Hartree-Fock (HF) approximation [13, 23]. By contrast, the Random Phase Approximation (RPA) gives $g_c \sim 0.7$ [12, 15]. Ref. [14] improved RPA by incorporating exchange correlations to find a considerably larger $g_c \sim 6$. The fixed-node Monte-Carlo calculation of Ref. [24] however did not find any evidence for the stripe phase. Moreover, mean field theory suggests a supersolid phase, i.e. the coexistence of the BCS and DW order, in a finite region of the phase diagram [25]. It remains unclear however whether the supersolid phase can survive quantum fluctuations.

These discrepancies and open questions highlight the challenges to develop an accurate theory for 2D dipolar Fermi gas. Ideally, the theory should have the following capabilities: (1) It keeps track of all many-body instabilities in the particle-particle and the particle-hole channel including the subtle interplay of the BCS and DW order for intermediate dipole tilting angles. (2) It extracts the momentum-dependent effective interactions between quasiparticles [26, 27] on the Fermi surface systematically from the bare dipolar interaction. (3) It takes into account thermal fluctuations to yield phase diagrams at low temperatures of interest to experiments. (4) It describes quantum fluctuations beyond HF and RPA.

In this letter, we present a theory that meets the requirements (1)-(4) above. It is based on functional renormalization group (FRG) [28, 29], a powerful many-body technique that gained considerable success in diverse systems including the Hubbard model [29, 30], the iron pnictides [29, 31], and ultracold quantum gases [32–37]. FRG can accurately predict the leading instability of the interacting fermions without a prior bias, making it the method of choice for problems with competing orders. Our FRG analysis maps out the phase diagram of the 2D dipolar Fermi gas at finite temperatures (Fig. 1) which include a Fermi liquid, a p -wave superfluid, and two distinct density wave phases outside the “collapse” region. In particular, FRG reveals a DW phase with nontrivial symmetry not found in the approaches summarized above.

Consider a continuum dipolar Fermi gas with chemical potential $\mu = E_F = p_F^2/2m$, where p_F is the Fermi momentum and m is the mass of the fermion. The dipole moment $\mathbf{d} = d\hat{\mathbf{d}}$ is aligned by external electric or magnetic field in the direction $\hat{\mathbf{d}} = (\sin\theta, 0, \cos\theta)$, i.e. tilted toward the x axis. The interaction between two dipoles separated by a distance \mathbf{r} is $V_{dd}(\mathbf{r}) = (d^2/r^3)[1 - 3(\hat{\mathbf{r}} \cdot \hat{\mathbf{d}})^2]$. Assume a tight harmonic confinement of frequency ω_z in the z direction, the effective interaction for two fermions within the xy plane has the form [38]

$$v(\mathbf{q}) = 2\pi d^2 |\mathbf{q}| [(\hat{\mathbf{q}} \cdot \hat{\mathbf{x}})^2 \sin^2 \theta - \cos^2 \theta] / \hbar, \quad (1)$$

where $\mathbf{q} = |\mathbf{q}|\hat{\mathbf{q}}$ is the in-plane momentum transfer. Note that Eq. (1) is only valid for $|\mathbf{q}| \leq \Lambda < \hbar/l_0$ where $l_0 = \sqrt{\hbar/m\omega_z}$ is the confinement length. We introduce the dimensionless interaction strength $g = md^2 p_F / \hbar^3$ as the product of the typical interaction $2\pi d^2 p_F / \hbar$ and the density of states $\nu = m/2\pi\hbar^2$. For brevity, we shall set \hbar and k_B to be unity below. Our goal is to find out which phase is stabilized given the temperature T , the dipole tilting angle θ , and the coupling strength g .

FRG implements Wilson's renormalization group for interacting fermions (see for example Ref. 39) in an exact and succinct fashion by flowing a generating functional, the average effective action $\Gamma_k[\bar{\psi}, \psi]$ where ψ and $\bar{\psi}$ are the fermionic fields, as a sliding momentum scale k is varied [29, 40–42]. Thermal and quantum fluctuations on different scales are separated by a device called the infrared regulator R_k and dealt with successively at each scale. We adopt Litim's optimized regulator [43],

$$R_k(\xi_{\mathbf{p}}) = [\text{sign}(\xi_{\mathbf{p}})k^2/2m - \xi_{\mathbf{p}}]\Theta(k^2/2m - |\xi_{\mathbf{p}}|), \quad (2)$$

where $\xi_{\mathbf{p}} = |\mathbf{p}|^2/2m - \mu$ is the bare dispersion, \mathbf{p} is the momentum within the xy plane, and Θ is the Heaviside step function. The evolution of Γ_k obeys the exact flow equation [29, 40, 44]

$$\partial_k \Gamma_k[\bar{\psi}, \psi] = -\frac{1}{2} \tilde{\partial}_k \text{Tr} \ln [\hat{\Gamma}_k^{(2)}[\bar{\psi}, \psi] + \hat{R}_k]. \quad (3)$$

Here $\hat{\Gamma}_k^{(2)}$ is the second order functional derivative of Γ_k with respect to the fermionic fields, $\tilde{\partial}_k$ means k -derivative only acting on $\hat{R}_k = i\hat{\sigma}_y R_k$, and Tr denotes integration over the imaginary time $\tau \in [0, 1/T]$, momentum \mathbf{p} , and trace over 2×2 matrices (denoted by hats) in the so-called superfield space. The coarse-grained functional Γ_k describes characteristic correlations up to scale k , with all higher energy fluctuations integrated out. At the bare scale Λ , $\Gamma_{k=\Lambda}$ coincides with the microscopic action. Thus, starting from the bare dispersion $\xi_{\mathbf{p}}$ and bare interaction $v(\mathbf{q})$ above and solving Eq. (3), one can obtain an effective theory $\Gamma_{k \rightarrow 0}$ for the low-energy collective behaviors of the interacting Fermi gas.

We expand Γ_k up to quartic order of ψ and $\bar{\psi}$,

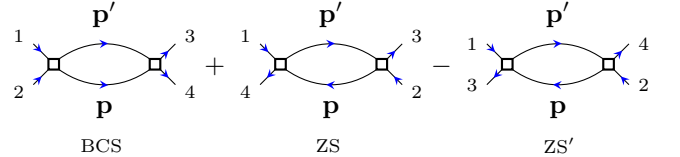
$$\Gamma_k = \bar{\psi}_1 G_k^{-1}(p_1) \psi_1 + \frac{1}{4} \Gamma_k^{(4)}(p_1, p_2, p_3) \bar{\psi}_4 \bar{\psi}_3 \psi_2 \psi_1 + \dots, \quad (4)$$

with the short hand notation $\psi_i = \psi(p_i)$, $p = (p^0, \mathbf{p})$ where the Matsubara frequency $p^0 = (2n+1)\pi T$. By momentum conservation $p_4 = p_1 + p_2 - p_3$ in the four-point vertex $\Gamma_k^{(4)}$. Repeated indices in Eq. (4) are summed over, i.e. $T \sum_{p^0} (2\pi)^{-2} \int d^2 \mathbf{p}$ is implied for each p_i . The inverse Green function is given by $G_k^{-1}(p) = ip^0 - \xi_{\mathbf{p}}^k - \Sigma_k(p)$ with $\xi_{\mathbf{p}}^k = \xi_{\mathbf{p}} + R_k(\xi_{\mathbf{p}})$ and Σ_k is the self-energy. Substituting Eq. (4) into Eq.(3) and neglecting higher order vertices, we obtain the coupled flow equations for $\Sigma_k(p)$ and $\Gamma_k^{(4)}(p_1, p_2, p_3)$ [35].

Next we make a few standard approximations so that the flow equations become numerically tractable. First, we neglect the p^0 dependence of $\Gamma_k^{(4)}$ and set the external Matsubara frequencies to be zero. Second, we assume $\Gamma_k^{(4)}$ only depends on the direction (not the magnitudes) of the momenta $\hat{\mathbf{p}}_1$, $\hat{\mathbf{p}}_2$ and $\hat{\mathbf{p}}_3$. This approximation is similar to projecting the momenta onto the Fermi surface in the widely used N-patch implementation of FRG for fermions on lattices. Finally, we ignore the self-energy Σ_k . With these assumptions, $\Gamma_k^{(4)}$ reduces to $\Gamma_k(\hat{\mathbf{p}}_1, \hat{\mathbf{p}}_2, \hat{\mathbf{p}}_3)$ which obeys the following flow equation

$$\begin{aligned} \partial_k \Gamma_k(\hat{\mathbf{p}}_1, \hat{\mathbf{p}}_2, \hat{\mathbf{p}}_3) = & \frac{1}{2} \int \frac{d\varphi_{\mathbf{p}}}{2\pi} \Gamma_k(\hat{\mathbf{p}}_1, \hat{\mathbf{p}}_2, \hat{\mathbf{p}}') \Gamma_k(\hat{\mathbf{p}}', \hat{\mathbf{p}}, \hat{\mathbf{p}}_3) \tilde{\partial}_k \Pi_k^+(\hat{\mathbf{p}}, \hat{\mathbf{p}}') \\ & + \int \frac{d\varphi_{\mathbf{p}}}{2\pi} \Gamma_k(\hat{\mathbf{p}}_1, \hat{\mathbf{p}}, \hat{\mathbf{p}}') \Gamma_k(\hat{\mathbf{p}}', \hat{\mathbf{p}}_2, \hat{\mathbf{p}}_3) \tilde{\partial}_k \Pi_k^-(\hat{\mathbf{p}}, \hat{\mathbf{p}}') \\ & - \int \frac{d\varphi_{\mathbf{p}}}{2\pi} \Gamma_k(\hat{\mathbf{p}}_1, \hat{\mathbf{p}}, \hat{\mathbf{p}}') \Gamma_k(\hat{\mathbf{p}}', \hat{\mathbf{p}}_2, \hat{\mathbf{p}}_4) \tilde{\partial}_k \Pi_k^-(\hat{\mathbf{p}}, \hat{\mathbf{p}}'), \end{aligned} \quad (5)$$

where the angular integral is over $\varphi_{\mathbf{p}}$, the polar angle of the 2D momentum \mathbf{p} . The three terms in Eq. (5) can be represented diagrammatically as



which are known as the BCS, the zero sound (ZS, or direct), and ZS' (or exchange) diagrams respectively. The internal momentum \mathbf{p}' is given by momentum conservation, $\mathbf{p}' = \mathbf{p}_1 + \mathbf{p}_2 - \mathbf{p}$ for BCS channel, $\mathbf{p}' = \mathbf{p} + \mathbf{p}_2 - \mathbf{p}_3$ for ZS channel, and $\mathbf{p}' = \mathbf{p} + \mathbf{p}_1 - \mathbf{p}_3$ for ZS' channel. The polarization bubbles in the particle-particle channel, Π_k^+ , and the particle-hole channel, Π_k^- , are given by

$$\Pi_k^{\pm}(\hat{\mathbf{p}}, \hat{\mathbf{p}}') = T \sum_{p^0} \int \frac{d|\mathbf{p}|^2}{4\pi} \frac{1}{(ip^0 - \xi_{\mathbf{p}}^k)} \frac{1}{(\mp ip^0 - \xi_{\mathbf{p}'}^k)}. \quad (6)$$

After performing the Matsubara summations analytically and the radial integral numerically in Eq. (6), we find that the main contribution to $\tilde{\partial}_k \Pi_k^{\pm}$ comes from the intersection area of two annuli in momentum space,

$$\tilde{\partial}_k \Pi_k^{\pm} = \pm \nu \int d\xi f_k(\xi, \pm \xi') \Theta(\tilde{k}^2 - |\xi|) \Theta(\tilde{k}^2 - |\xi'|), \quad (7)$$

where $\tilde{k} = k/\sqrt{2m}$, $\xi = \xi_{\mathbf{p}}$, $\xi' = \xi_{\mathbf{p}'}$, and the weight function $f_k(\xi, \xi') = [x_k/2 \cosh^2(x_k/2) - \tanh(x_k/2)]/\tilde{k}^3$ for $\xi\xi' > 0$ and $f_k(\xi, \xi') = -x_k^2 \tanh(x_k)/[2 \cosh^2(x_k)\tilde{k}^3]$ for $\xi\xi' < 0$ in terms of $x_k = k^2/2mT$. The vertex function at scale Λ is the antisymmetrized bare interaction,

$$\Gamma_{\Lambda}(\hat{\mathbf{p}}_1, \hat{\mathbf{p}}_2, \hat{\mathbf{p}}_3) = \frac{1}{2} [v(\hat{\mathbf{p}}_3 - \hat{\mathbf{p}}_1) - v(\hat{\mathbf{p}}_2 - \hat{\mathbf{p}}_3)]. \quad (8)$$

Eqs. (5)-(8) are the main analytical results of our paper.

We solve the flow Eq. (5) with the initial condition (8) numerically by discretizing the sliding scale $k \in [0, \Lambda]$ and the polar angle $\varphi_{\mathbf{p}} \in [0, 2\pi]$. We choose $\Lambda = 0.4p_F$, which corresponds to an energy scale much larger than T [45, 46], and an angular grid of $N = 48$ patches. The evolution of $\Gamma_k(\hat{\mathbf{p}}_1, \hat{\mathbf{p}}_2, \hat{\mathbf{p}}_3)$, which contains $N^3 = 110592$ running coupling constants, is monitored as k is reduced from Λ toward 0. To identify the many-body instabilities, we introduce the standard coupling matrices in various channels [31, 47], e.g. $V_Q(\hat{\mathbf{p}}_1, \hat{\mathbf{p}}_2)$ by setting $\mathbf{p}_3 = \mathbf{p}_1 + \mathbf{Q}$ in Γ_k for given \mathbf{Q} . It turns out the leading instability occurs either in the particle-particle channel with the coupling matrix $V_{BCS}(\hat{\mathbf{p}}_1, \hat{\mathbf{p}}_2) = [\Gamma_k(\hat{\mathbf{p}}_1, -\hat{\mathbf{p}}_1, \hat{\mathbf{p}}_2) + \Gamma_k(\hat{\mathbf{p}}_2, -\hat{\mathbf{p}}_2, \hat{\mathbf{p}}_1)]/2$ or in the particle-hole channel with the coupling matrix $V_{DW}(\hat{\mathbf{p}}_1, \hat{\mathbf{p}}_2) = [\Gamma_k(\hat{\mathbf{p}}_1, \hat{\mathbf{p}}_2, \hat{\mathbf{p}}_1) + \Gamma_k(\hat{\mathbf{p}}_2, \hat{\mathbf{p}}_1, \hat{\mathbf{p}}_2)]/2$.

Each channel coupling matrix V is diagonalized to find its eigenvalues and eigenvectors, $\int \frac{d\varphi_2}{2\pi} V(\varphi_1, \varphi_2) \Psi(\varphi_2) = \lambda_k \Psi(\varphi_1)$, where we have used the unit vector $\hat{\mathbf{p}}_i$ and its corresponding polar angle φ_i interchangeably. For given (θ, g, T) , if Γ_k develops no singular behavior as k is reduced, the gas is in the normal phase. If some λ_k values diverge, the Fermi liquid is unstable. The most diverging λ_k points to the channel in which the leading instability occurs, while its eigenvector $\Psi(\varphi)$ yields the symmetry of the incipient long-range order. We define the critical scale Λ_c as the value of k when the largest element of $\Gamma_k(\hat{\mathbf{p}}_1, \hat{\mathbf{p}}_2, \hat{\mathbf{p}}_3)$ exceeds $10^2 E_F$. It serves as a rough estimation of the critical temperature T_c of the corresponding broken symmetry phase.

Identifying the instability in the particle-hole channel for a Fermi gas with circular Fermi surface requires some care. V_{DW} may look like the $\mathbf{Q} \rightarrow 0$ limit of V_Q . It however can be equivalently viewed as two fermions exchanging momentum, $(\mathbf{p}_1, \mathbf{p}_2) \rightarrow (\mathbf{p}_2, \mathbf{p}_1)$, with a finite momentum transfer $\mathbf{Q}' = \mathbf{p}_2 - \mathbf{p}_1$, due to the antisymmetry of the vertex. In particular, scattering across the Fermi surface, $(\mathbf{p}_1, -\mathbf{p}_1) \rightarrow (-\mathbf{p}_1, \mathbf{p}_1)$, drives a DW (stripe) order with ordering wave vector $|\mathbf{Q}'| = 2p_F$ [16]. Within our FRG scheme, we find that while the DW order does have a dominant \mathbf{Q}' component, it cannot be characterized by a single wave vector [23].

Fig. 1a shows the phase diagram of 2D dipolar Fermi gas for $T = 0.01E_F$. It features four phases: the Fermi liquid (FL), the BCS superfluid phase dominated by p_x -wave symmetry, and two distinctive DW phases. For completeness, we also indicated the “collapse” region ob-

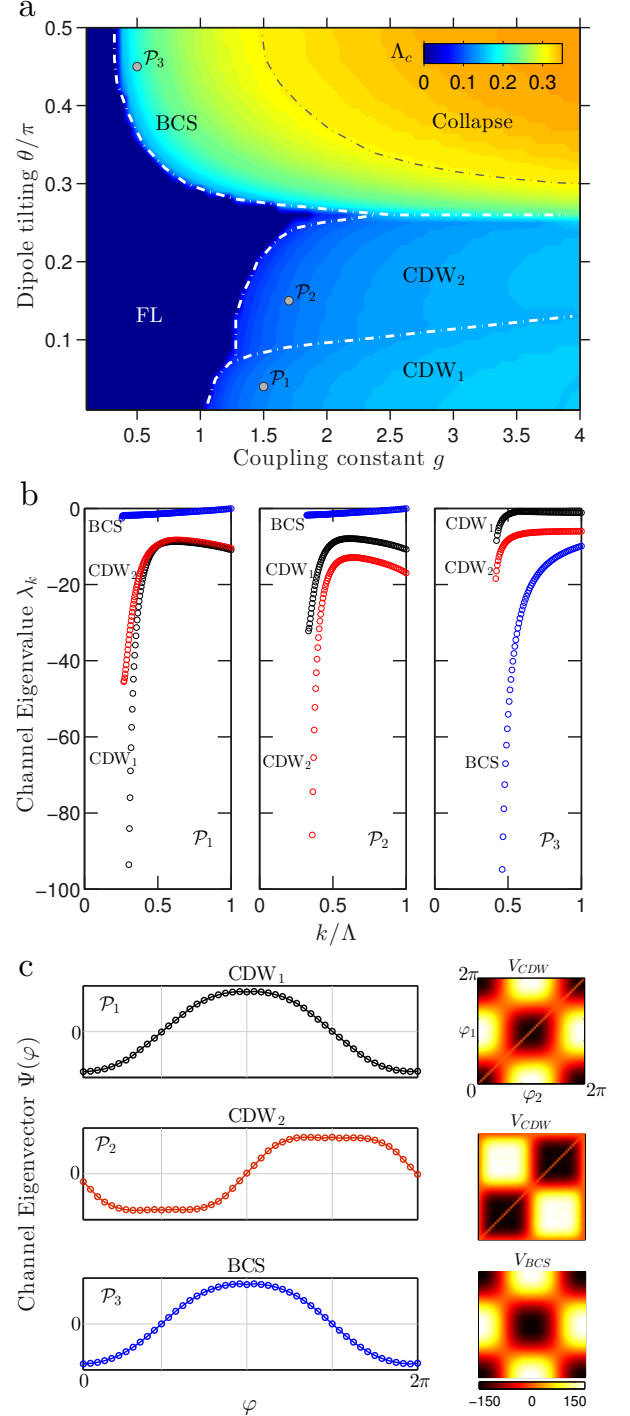


FIG. 1. (Color online) a) The phase diagram of two-dimensional spinless dipolar Fermi gas at $T = 0.01E_F$ predicted by FRG. It displays a Fermi liquid (FL), a p -wave superfluid (BCS) and two distinct density wave phases, DW₁ and DW₂. The colormap shows the critical scale Λ_c at which the vertex diverges (see the main text). Three representative points \mathcal{P}_1 , \mathcal{P}_2 and \mathcal{P}_3 on the phase diagram are chosen to show the details of the FRG flow. b) The flows of the largest eigenvalue of V_{BCS} and the two largest eigenvalues of V_{DW} corresponding to the DW₁ and DW₂ order respectively. c) The eigenvectors of the leading instability and the corresponding channel matrices near the end of the flow.

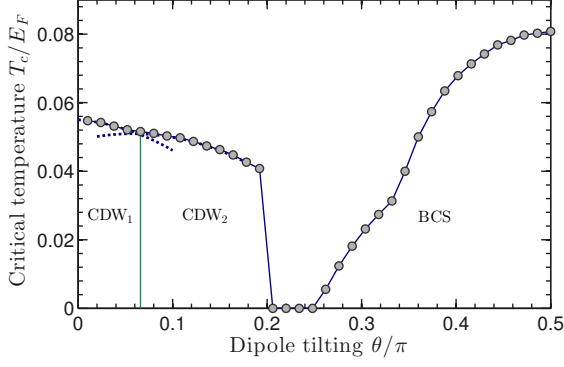


FIG. 2. The critical temperature T_c as a function of the dipole tilting angle θ for fixed interaction $g = 1.5$ estimated from the FRG flow. Dashed lines are the extensions of the fits to the data points in the DW₁ and DW₂ region, respectively.

tained by the same procedure as Ref. [23]. Three points on the (θ, g) plane, \mathcal{P}_1 , \mathcal{P}_2 and \mathcal{P}_3 , are chosen to represent the DW₁, DW₂, and BCS phase respectively. Their corresponding λ_k , $\Psi(\varphi)$, and $V(\varphi_1, \varphi_2)$ are shown in Fig. 1b-1c.

Several features of Fig. 1a are in qualitative agreement with previous phase diagrams in Refs. [14, 20, 23, 25]. For example, the BCS phase emerges beyond a critical dipole tilting angle $\theta_c \approx 0.26\pi$, while the DW order only develops beyond a critical coupling, e.g. $g_c = 1.1$ for $\theta = 0$. Fig. 1a shows that the BCS phase undergoes a direct transition to DW₂ instead of through an intermediate, coexisting phase. Within our implementation of FRG, the leading instability always occurs either in the BCS or the DW channel. The case of degenerately diverging λ_k in both channels is never observed, so there is no evidence for a supersolid phase. We can identify DW₂ as the stripe density wave discussed previously with a density modulation along the y axis with period $\sim \hbar/2p_F$. As shown in Fig. 1c, the effective interaction V_{DW} is repulsive and diverging near the region $\hat{\mathbf{p}}_1 \sim -\hat{\mathbf{p}}_2 \sim \hat{y}$, favoring the dominant ordering wave vector $\mathbf{Q}' = 2p_F\hat{y}$. Note that $\Psi(\varphi)$ vanishes for $\varphi = 0$ and π , i.e. there is no modulation along the x direction.

Our most significant finding is the DW₁ phase seen for smaller dipolar tilting angles θ . From the eigenvector $\Psi(\varphi)$, it is clear that the two DW phases are roughly related to each other by a $\pi/2$ rotation. The density modulation is thus along the x axis in the DW₁ phase. In contrast to DW₂, the DW₁ order is not expected from the bare interaction $v(\mathbf{q})$ which is almost isotropic for small θ . Only under the FRG flow does the effective interaction vertex V_{DW} become increasingly anisotropic and drastically different from the bare interaction. As k is reduced, the renormalized interaction for two fermions with $\hat{\mathbf{p}}_1 \sim -\hat{\mathbf{p}}_2 \sim \hat{x}$ grows dominantly repulsive and eventually diverges. While the translational symmetry

breaking along the x direction is counter-intuitive, a DW order along \hat{y} in the limit of $\theta \rightarrow 0$, as previously believed, seems implausible because all directions of \mathbf{Q}' are energetically degenerate.

Single channel renormalization group [39] and RPA are widely used in the study 2D Fermi liquids, and their deficiencies have been noticed [46, 48]. Neglecting the ZS' channel (as in RPA) will violate the antisymmetry in the forward scattering vertex [46]. Strong interference between ZS and ZS' near the zero angle $\hat{\mathbf{p}}_1 \sim \hat{\mathbf{p}}_2$ leads to small angle anomalies and invalidates the ladder approximation [46]. The interference between the BCS and ZS channel (relevant to the putative supersolid phase) become important when $\hat{\mathbf{p}}_1 \sim -\hat{\mathbf{p}}_2$ [39, 48]. The FRG approach described here is capable of describing these subtle interplays between the BCS, ZS, and ZS' channels, and the antisymmetry of Γ_k is respected throughout.

Now we comment on the requirements to observe the broken symmetry phases experimentally. Fig. 1a suggests that to access the BCS phase at $T \sim 0.01E_F$, which is much lower than the temperatures $T \sim 0.2E_F$ achieved for Dy [1] and Er [2] gases, one needs go to relatively strong interactions $g > 0.5$. For the NaK gas reported in Ref. [6], g is on the order of 1.34 with $d = 0.8$ Debye and area density of $4 \times 10^7 \text{ cm}^{-2}$. In principle, d can be further increased to 2.7 Debye, giving a ten-fold increase in g . At higher temperatures, the phase boundaries are shifted to the right by thermal fluctuations, so stronger interactions are required to reach the BCS and DW phases. The (color-coded) Λ_c values in Fig. 1a provides a rough guide for the T_c . Note the T_c of the BCS phase is typically higher than that of the DW phases. A more accurate estimation of T_c is shown in Fig. 2 for fixed $g = 1.5$ as a function of θ . It is obtained by solving the flow equation at different T for given (θ, g) and identifying T_c as the temperature at which a divergence in Γ_k develops. We observe that T_c can be 5 to 10 percent of E_F .

Our instability analysis is confined within the normal phase, it does not directly describe the broken symmetry phases including the proliferation of topological defects which tends to suppress T_c to values much lower than estimated here. The Kosterlitz-Thouless transition of the stripe (DW₂) phase has been described in Ref. [49]. It would be interesting to perform a similar analysis of all candidate phases found here. The accuracy of our results can be improved by including the full momentum dependence in $\Gamma_k^{(4)}$ and Σ_k in the FRG flow. For example, we expect the Fermi surface deformations [27, 50–52] due to the self-energy correction may slightly reduce the region of the DW₁ phase and enhance the stability of the supersolid. Such calculation is numerically much more demanding and reserved for future work. We hope the results reported here can stimulate further application of FRG to interacting Fermi gases including spin 1/2 dipolar Fermi gases [11, 53, 54].

E.Z. is grateful to Xiaopeng Li, Ludwig Mathey, Shan-

Wen Tsai, and Ryan Wilson for many helpful discussions. This work is supported by the NSF Grant No. PHY-1205504 and the AFOSR Grant No. FA9550-16-1-0006. A.K. is also supported by U.S. ARO Grant No. W911NF-11-1-0230.

-
- [1] M. Lu, N. Q. Burdick, and B. L. Lev, *Phys. Rev. Lett.* **108**, 215301 (2012).
 - [2] K. Aikawa, A. Frisch, M. Mark, S. Baier, R. Grimm, and F. Ferlaino, *Phys. Rev. Lett.* **112**, 010404 (2014).
 - [3] B. Naylor, A. Reigues, E. Maréchal, O. Gorceix, B. Laburthe-Tolra, and L. Vernac, *Phys. Rev. A* **91**, 011603 (2015).
 - [4] K.-K. Ni, S. Ospelkaus, M. H. G. de Miranda, A. Pe'er, B. Neyenhuis, J. J. Zirbel, S. Kotochigova, P. S. Julienne, D. S. Jin, and J. Ye, *Science* **322**, 231 (2008).
 - [5] S. Ospelkaus, K.-K. Ni, M. H. G. de Miranda, B. Neyenhuis, D. Wang, S. Kotochigova, P. S. Julienne, D. S. Jin, and J. Ye, *Faraday Discuss.* **142**, 351 (2009).
 - [6] J. W. Park, S. A. Will, and M. W. Zwierlein, *Phys. Rev. Lett.* **114**, 205302 (2015).
 - [7] J. W. Park, S. A. Will, and M. W. Zwierlein, *New Journal of Physics* **17**, 075016 (2015).
 - [8] C.-H. Wu, J. W. Park, P. Ahmadi, S. Will, and M. W. Zwierlein, *Phys. Rev. Lett.* **109**, 085301 (2012).
 - [9] M. Baranov, M. Dalmonte, G. Pupillo, and P. Zoller, *Chemical Reviews* **112**, 5012 (2012).
 - [10] M. A. Baranov, *Physics Reports* **464**, 71 (2008).
 - [11] Y. Li and C. Wu, *Journal of Physics: Condensed Matter* **26**, 493203 (2014).
 - [12] Y. Yamaguchi, T. Sogo, T. Ito, and T. Miyakawa, *Phys. Rev. A* **82**, 013643 (2010).
 - [13] M. Babadi and E. Demler, *Phys. Rev. B* **84**, 235124 (2011).
 - [14] M. M. Parish and F. M. Marchetti, *Phys. Rev. Lett.* **108**, 145304 (2012).
 - [15] K. Sun, C. Wu, and S. Das Sarma, *Phys. Rev. B* **82**, 075105 (2010).
 - [16] J. K. Block and G. M. Bruun, *Phys. Rev. B* **90**, 155102 (2014).
 - [17] J. K. Block, N. T. Zinner, and G. M. Bruun, *New Journal of Physics* **14**, 105006 (2012).
 - [18] B. P. van Zyl, W. Kirkby, and W. Ferguson, *Phys. Rev. A* **92**, 023614 (2015).
 - [19] L. You and M. Marinescu, *Phys. Rev. A* **60**, 2324 (1999).
 - [20] G. M. Bruun and E. Taylor, *Phys. Rev. Lett.* **101**, 245301 (2008).
 - [21] M. A. Baranov, M. S. Mar'enko, V. S. Rychkov, and G. V. Shlyapnikov, *Phys. Rev. A* **66**, 013606 (2002).
 - [22] C. Zhao, L. Jiang, X. Liu, W. M. Liu, X. Zou, and H. Pu, *Phys. Rev. A* **81**, 063642 (2010).
 - [23] L. M. Sieberer and M. A. Baranov, *Phys. Rev. A* **84**, 063633 (2011).
 - [24] N. Matveeva and S. Giorgini, *Phys. Rev. Lett.* **109**, 200401 (2012).
 - [25] Z. Wu, J. K. Block, and G. M. Bruun, *Phys. Rev. B* **91**, 224504 (2015).
 - [26] Z.-K. Lu and G. V. Shlyapnikov, *Phys. Rev. A* **85**, 023614 (2012).
 - [27] C.-K. Chan, C. Wu, W.-C. Lee, and S. Das Sarma, *Phys. Rev. A* **81**, 023602 (2010).
 - [28] P. Kopietz, L. Bartosch, and F. Schütz, *Introduction to the functional renormalization group*, Vol. 798 (Springer Science & Business Media, 2010).
 - [29] W. Metzner, M. Salmhofer, C. Honerkamp, V. Meden, and K. Schönhammer, *Rev. Mod. Phys.* **84**, 299 (2012).
 - [30] D. Zanchi and H. J. Schulz, *Phys. Rev. B* **61**, 13609 (2000).
 - [31] C. Platt, W. Hanke, and R. Thomale, *Advances in Physics* **62**, 453 (2013).
 - [32] L. Mathey, S.-W. Tsai, and A. H. Castro Neto, *Phys. Rev. Lett.* **97**, 030601 (2006).
 - [33] L. Mathey, S.-W. Tsai, and A. H. Castro Neto, *Phys. Rev. B* **75**, 174516 (2007).
 - [34] I. Boettcher, J. M. Pawłowski, and C. Wetterich, *Phys. Rev. A* **89**, 053630 (2014).
 - [35] Y. Tanizaki, G. Fejős, and T. Hatsuda, *Progress of Theoretical and Experimental Physics* **2014** (2014).
 - [36] S. G. Bhongale, L. Mathey, S.-W. Tsai, C. W. Clark, and E. Zhao, *Phys. Rev. Lett.* **108**, 145301 (2012).
 - [37] S. G. Bhongale, L. Mathey, E. Zhao, S. F. Yelin, and M. Lemeshko, *Phys. Rev. Lett.* **110**, 155301 (2013).
 - [38] U. R. Fischer, *Phys. Rev. A* **73**, 031602 (2006).
 - [39] R. Shankar, *Rev. Mod. Phys.* **66**, 129 (1994).
 - [40] C. Wetterich, *Physics Letters B* **301**, 90 (1993).
 - [41] T. R. Morris, *International Journal of Modern Physics A* **09**, 2411 (1994).
 - [42] J. Polchinski, *Nuclear Physics B* **231**, 269 (1984).
 - [43] D. F. Litim, *Physics Letters B* **486**, 92 (2000).
 - [44] J. Berges, N. Tetradis, and C. Wetterich, *Physics Reports* **363**, 223 (2002).
 - [45] G. Y. Chitov and D. Sénéchal, *Phys. Rev. B* **52**, 13487 (1995).
 - [46] G. Y. Chitov and D. Sénéchal, *Phys. Rev. B* **57**, 1444 (1998).
 - [47] H. Zhai, F. Wang, and D.-H. Lee, *Phys. Rev. B* **80**, 064517 (2009).
 - [48] N. Dupuis, *The European Physical Journal B* **3**, 315 (1998).
 - [49] Z. Wu, J. K. Block, and G. M. Bruun, arXiv preprint arXiv:1509.02679 (2015).
 - [50] K. Aikawa, S. Baier, A. Frisch, M. Mark, C. Ravensbergen, and F. Ferlaino, *Science* **345**, 1484 (2014).
 - [51] T. Miyakawa, T. Sogo, and H. Pu, *Phys. Rev. A* **77**, 061603 (2008).
 - [52] J.-N. Zhang and S. Yi, *Phys. Rev. A* **80**, 053614 (2009).
 - [53] S. G. Bhongale, L. Mathey, S.-W. Tsai, C. W. Clark, and E. Zhao, *Phys. Rev. A* **87**, 043604 (2013).
 - [54] E. G. C. P. van Loon, M. I. Katsnelson, and M. Lemeshko, *Phys. Rev. B* **92**, 081106 (2015).